NOAA Technical Report ERL 391–SEL 39

Photodissociation Rates for Minor Species in the Earth's Atmosphere

R. D. Harris
R. A. McCue
G. W. Adams

September 1977

U.S. DEPARTMENT OF COMMERCE
National Oceanic and Atmospheric Administration
Environmental Research Laboratories

NOAA Technical Report ERL 391–SEL 39

Photodissociation Rates for Minor Species in the Earth's Atmosphere

R. D. Harris
R. A. McCue
G. W. Adams

Space Environment Laboratory
Boulder, Colorado

September 1977

U.S. DEPARTMENT OF COMMERCE
Juanita M. Kreps, Secretary

National Oceanic and Atmospheric Administration
Richard A. Frank, Administrator

Environmental Research Laboratories
Wilmot Hess, Director

CONTENTS

PHOTODISSOCIATION RATES FOR MINOR SPECIES IN THE EARTH'S ATMOSPHERE

R. D. Harris*, R. A. McCue*, and G. W. Adams

ABSTRACT. Photodissociation rates per molecule for ten minor atmospheric species have been computed as functions of wavelength, altitude, and solar zenith angle for medium solar activity. Calculations for wavelengths from the onset of dissociation to 1000 Å and for altitudes below 110 km for CO, CO_2, CH_4, C_2H_4, NO, NO_2, N_2O, H_2O, H_2O_2, HNO_3, and the major species O_3 and O_2 are reported. Photodissociation calculations depend upon the atmospheric O_2 and O_3 absorption but are independent of specific minor species densities.

1. INTRODUCTION

Recent interest in stratospheric contaminants and their possible effects on the ozone population has sparked both theoretical and experimental efforts to identify and generate accurate height profiles for all atmospheric species. Many chemical species that constitute only a minute fraction of the total air population have been found to be extremely important in the chemistry of both the mesosphere and stratosphere. Accurate photodissociation rates of these minor species are a necessary ingredient in the chemical-kinetic models that attempt to describe those complex reactions. This report presents calculations of photodissociation rates (per molecule) for minor species in the Earth's atmosphere as functions of wavelength, altitude, and solar zenith angle. Our motivation lies in the fact that the solar flux penetrating the atmosphere is absorbed primarily by O_2 and O_3; the photodissociation rate (per molecule) of minor species, N_2O for example, can be calculated independent of the N_2O density. Thus, our calculations are based on experimental densities of O_2 and O_3 and measured cross sections that are mostly well known. The modeler who must use dissociation rates is then free to choose minor density profiles of his own particular bias.

Although the absorption cross sections for a number of important species have been measured with great detail, the cross sections of other species mostly of recent interest have not yet been measured and we have not yet calculated p-d rates for them. The minor species included in this report are: CO, CO_2, CH_4, C_2H_4, NO, NO_2, N_2O, H_2O, H_2O_2, and HNO_3. Cross sections and dissociation rates are presented in separate sections. Calculations for the major species O_2 and O_3 as functions of height and zenith angle are also given for easy reference.

*Center for Research in Aeronomy, Utah State University, Logan, Utah 84322.

2. CALCULATIONS

The photodissociation rates for species i were calculated as

$$j_i(\lambda_1, \lambda_2, \chi, z) = \int_{\lambda_1}^{\lambda_2} \sigma_i(\lambda)\phi_\infty(\lambda) \exp - \sum_m \sigma_m(\lambda) N_m(\chi, z) d_\lambda$$

where i denotes minor species,

m denotes major species,

j_i is the dissociation rate per molecule of species i (sec^{-1}),

λ_1 and λ_2 are the wavelengths bounding the region of interest,

χ is the zenith angle of the Sun,

z is the altitude,

σ_i (σ_m) is the photon absorption cross section of species i (m),

ϕ_∞ is the solar flux at the top of the atmosphere, and

$N_m(\chi, z)$ is the column density of species m along the path from altitude z to the Sun at zenith angle χ.

For the dissociation curves to be utilized j_i must be multiplied by the density. This gives the total photodissociation rate $j_i = n_i j_i$ (ion-pairs/cm^3−sec).

The "major" species are O_2 and O_3, since these are the species that control the solar flux that penetrates into the middle and lower atmosphere in the wavelengths of interest here. The ionization limit of O_2 is at 1027.5 Å, so wavelengths short of this are predominantly absorbed high in the thermosphere. Absorption by minor species is usually not of interest above 120 km; therefore calculations have been limited to altitudes below 110 km, and wavelengths longer than 1000 Å. The O_2 density profile was taken from the *U.S. Standard Atmosphere* [1962] for 0 to 90 km, and from the Jacchia [1971] model for 90 to 120 km. Since the solar flux absorption depends on the total column content, the dissociation rates at 110 km are essentially independent of the major species densities above 120 km. Atmospheric parameters are given in Table 1. The O_2 absorption cross sections are plotted in Figure 1. Following are the O_2 absorption cross sections used:

1100–1030 Å: Cross sections are from Hinteregger [1965].

1030–1280 Å: Cross sections used in this region are from Adams [1974], which are band-averaged in 10 Å steps following Hudson and Mahle [1972].

1280–1750 Å (Schumann-Runge continuum): The results summarized in Hudson's [1971] review are used, since there is good agreement between the different measurements.

1750–2050 Å (Schumann-Runge bands): Hudson and Mahle's [1972] band-averaged cross sections were used here.

2050–2500 Å (Herzberg continuum): Cross sections in this region are from Ditchburn and Young [1962]. Absorption in this wavelength region can energetically lead only to two ground-state atomic oxygen atoms, which is spin-forbidden, so cross sections in the Herzberg continuum are small.

The ozone profile is not as "standard" as either O_2 or N_2, and it is not clear which of the many values available is most correct. The solar radiation below 1750 Å is absorbed overwhelmingly by O_2. (At 65 km the solar flux in these wavelengths has been reduced more than four orders of magnitude.) CO, CH_4, and C_2H_4 are dissociated entirely in this region. In the Schumann-Runge bands, 1750–2050 Å, the atmosphere is almost transparent down to 50 km; at 30 km the O_2 absorption is 1–4 times the O_3 absorption, depending on the O_3 density assumed. The species NO, H_2O, and O_2 are examples of species whose dissociation rate below about 60–70 km is primarily dependent

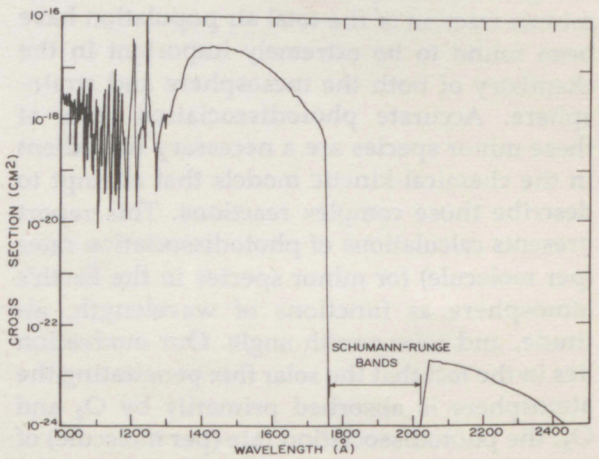

Figure 1. Experimental O_2 absorption cross section vs. wavelength.

on the solar flux in the Schumann-Runge band wavelengths. For wavelengths greater than 2050 Å the absorption is primarily O_3. The 2000–3000 Å region of O_3 (the Hartley band and continuum) is especially important since it overlies the weak Herzberg continuum of O_2. Carbon dioxide, N_2O, and HNO_3 have about equal contributions to their dissociation rates from the 1750–2050 Å band and from wavelengths greater than 2050 Å. NO_2, H_2O_2, and O_3 have the major portion of their dissociation rates beyond 2500 Å.

To illustrate the effects of ozone variability on dissociation rates, a number of both experimental and theoretical O_3 profiles were collected [Evans, 1967; Shimazaki and Ogawa, 1974; Wofsy, 1974; Grobecker, 1975; Nicolet, 1975; Riegler et al., 1976], from which could be estimated minimum and maximum bracketing values for the O_3 density. These bracketing values, plotted in Figure 2a, were used to calculate the H_2O_2 dissociation rate in Figure 2b. Figures 2c and 2d show the dissociation rates for O_3 and NO_2, for low– and mid–O_3 profiles. These figures illustrate the sensitivity or rather insensitivity of dissociation rates to O_3 densities. Despite the very large variation in O_3 (Figure 2a) for an overhead Sun, a variation in O_3 produces differences only in the photodissociation rate below 45 km. Dissociation rates at large zenith angles show the effects of an O_3 variation at much higher altitudes because of the large O_3 column densities, but then the rates fall off rather rapidly.

The O_3 density profiles used for the detailed dissociation rate calculations were taken from Adams and Megill [1970] for altitudes between 29 and 120 km, and from Dutsch and Mateer

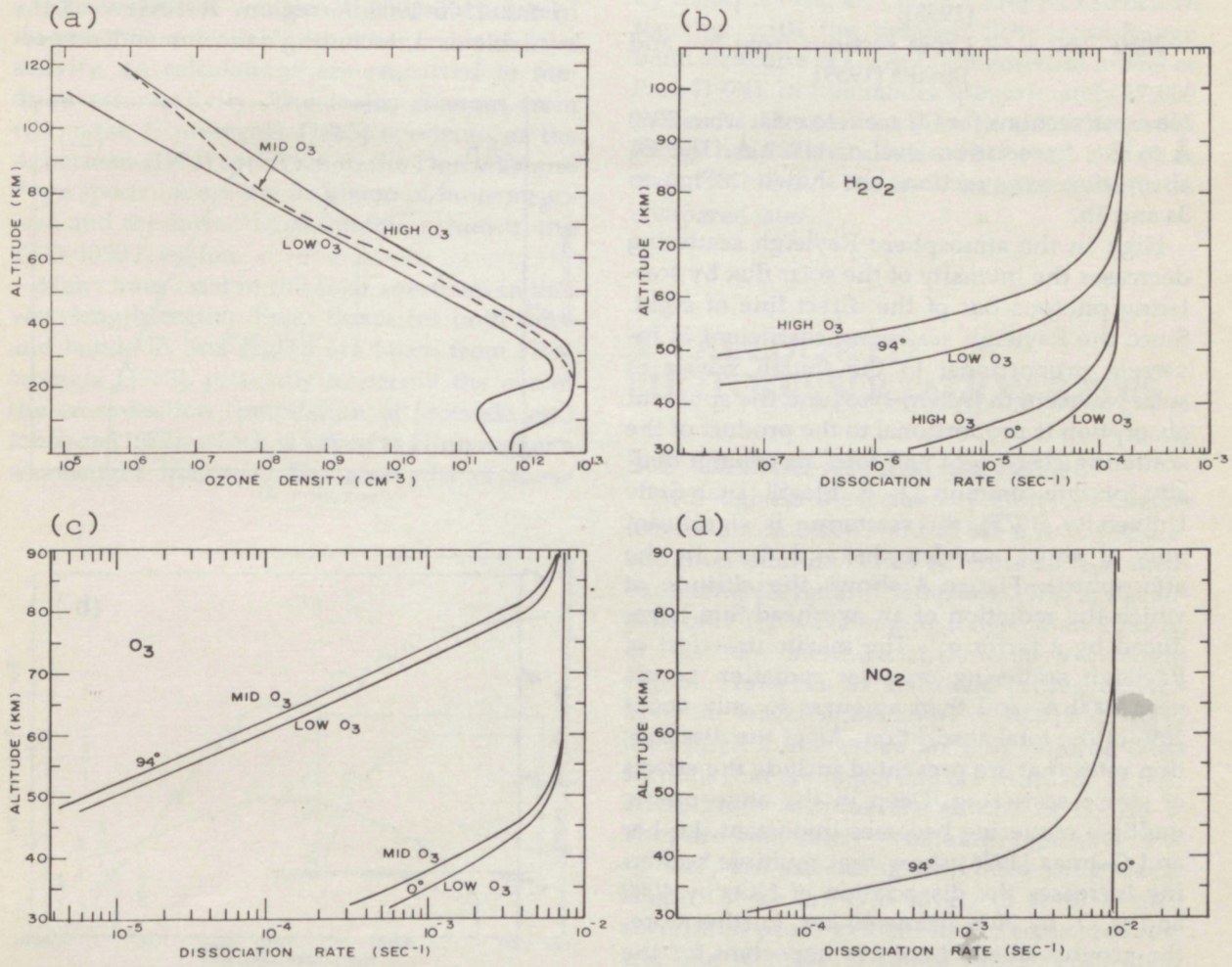

Figure 2. (a) Extreme values for O_3 profiles based on collected O_3 data; (b) H_2O_2 dissociation rates based on high and low O_3 profiles from (a); (c,d) O_3 and NO_2 photodissociation rates based on middle and low O_3 profiles of (a).

Table 1.
Model Atmosphere Parameters

z (km)	T (K)	$[0_2]$ (cm^{-3})	$\int_z^\infty n(0_2)dz$ (cm^{-2})	$[0_3]$ (cm^{-3})	$\int_z^\infty n(0_3)dz$ (cm^{-2})
110	257	4.34 + 11*	2.29 + 17	2.0 + 6	1.15 + 12
100	210	2.17 + 12	1.29 + 18	7.5 + 6	5.36 + 12
90	180.6	1.38 + 13	7.51 + 18	2.1 + 7	1.82 + 13
80	180.7	8.7 + 13	4.77 + 19	1.0 + 8	6.61 + 13
70	219.7	3.81 + 14	2.53 + 20	5.6 + 8	3.36 + 14
60	255.8	1.35 + 15	1.02 + 21	4.1 + 9	2.21 + 15
50	273.6	4.47 + 15	3.63 + 21	3.6 + 10	1.68 + 16
40	250.3	1.74 + 16	1.30 + 22	6.0 + 11	1.87 + 17
30	226.5	8.02 + 16	5.42 + 22	6.0 + 12	3.53 + 18
20	216.6	3.87 + 17	2.49 + 23	3.5 + 12	8.30 + 18
10	223.3	1.80 + 18	1.19 + 24	5.0 + 11	1.05 + 19
0	288.1	5.33 + 18	4.53 + 24	1.0 + 8	1.06 + 19

*4.34 + 11 = 4.34 × 10″

[1964] for altitudes between 0 and 28 km (Table 1). The following O_3 absorption cross sections were used:

1050–2050 Å — Cross sections given by Tanaka, Inn, and Watanabe [1953];

2050–7560 Å — Cross sections from Inn and Tanaka [1959].

No cross sections for O_3 seem to exist from 7560 Å to the dissociation level of 11929 Å. The O_3 absorption cross sections are shown in Figures 3a and 3b.

High in the atmosphere Rayleigh scattering decreases the intensity of the solar flux by scattering photons out of the direct line of sight. Since the Rayleigh scattering coefficient is inversely proportional to the fourth power of solar wavelength [Allen, 1963] and the apparent absorption is proportional to the product of the scattering coefficient and total air column density [private commun., L. R. Megill, Utah State University, 1975], the scattering is significant only at short wavelengths and deep in the atmosphere. Figure 4 shows the altitude at which the radiation of an overhead Sun is reduced by a factor e^{-1}. The maximum effect of Rayleigh scattering on solar radiation occurs near 2000 Å, and then amounts to only about 20% of the total absorption. All of the dissociation rates that are presented include the effects of single scattering. Deep in the atmosphere, multiple scattering becomes important. Luther and Gelinas [1976] show that multiple scattering increases the dissociation of NO_2 by 40% and of O_3 by 30% below 40 km. Furthermore, the ground albedo becomes important for the wavelengths that penetrate to the ground. Multiple scattering effects are beyond the scope of this paper, so results given for altitudes below 40 km should be used with appropriate caution.

There is considerable uncertainty and disagreement about the magnitude of the solar fluxes in some wavelength regions, particularly in the 1300–1900 Å region. A review of the available data, including a recommended spec-

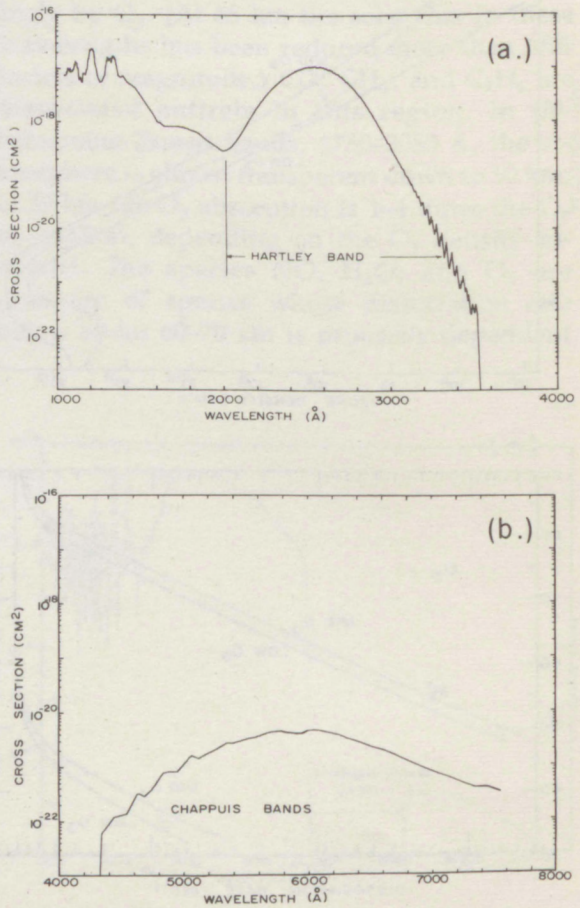

Figure 3. Experimental O_3 absorption cross section (a) from 1000 to 4000 Å, and (b) from 4000 to 8000 Å.

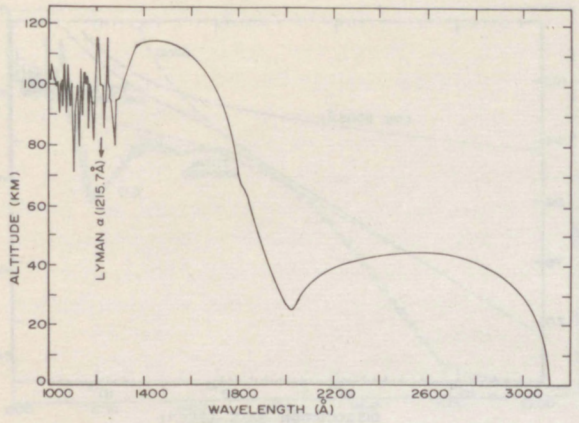

Figure 4. Altitude at which $\phi = \phi_\infty e^{-1}$; direct solar radiation for an overhead Sun has been reduced by 37%.

trum for medium solar activity, has been prepared by Donnelly and Pope [1973]; that spectrum is used here for wavelengths longer than 1300 Å (Fig. 5). Hinteregger's [1970] spectrum is used for shorter wavelengths. Unfortunately, no spectra are available for other levels of solar activity, so calculations are restricted to medium solar activity. The major changes from either the Hinteregger [1965] spectrum or the Ackerman [1971] spectrum to the Donnelly and Pope spectrum are the inclusion of more structure and the lowering of the flux values in the 1300–1800 Å region.

Many lines exist in the solar spectrum in this wavelength region. Solar fluxes for both lines and bands in this region are taken from Hinteregger [1970], primarily to permit the use of the cross-section compilation of Stolarski and Johnson [1972], which is keyed to Hinteregger's wavelength intervals. The strengths of these lines are represented by the arrow tips in Figure 5.

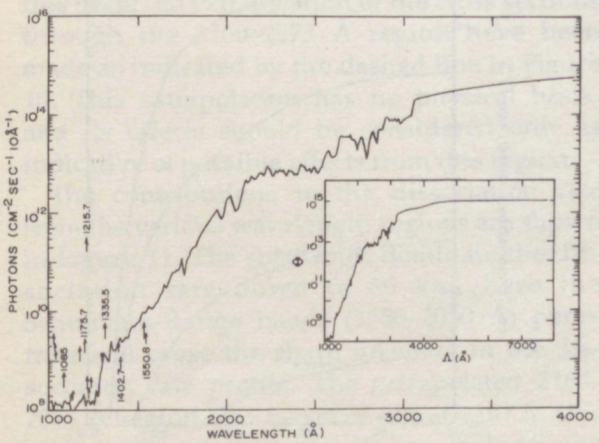

Figure 5. Solar flux values used in the dissociation calculations.

For most species and spectral regions, the photon absorption cross sections are relatively smooth and the calculations are straightforward. Nevertheless, all of the detail in the published cross sections is included in the calculations. The Schumann-Runge bands (1750–2050 Å) of O_2 are intensely structured, but for minor species whose cross sections are smoothly varying in this region, Hudson and Mahle's [1972] band-averaged O_2 cross sections are adequate. However, two of the minor species, CO_2 and NO, have moderately structured cross sections in the Schumann-Runge band region. The dissociation rates for these two species were handled by averaging the CO_2 and NO cross sections over the wavelength intervals keyed to the band-averaged O_2 cross sections of Hudson and Mahle [1972], and also by incorporating all the CO_2 and NO structure together with the detailed Schumann-Runge band structure of O_2 in the theoretical model of Park [1974]. In this model approximately 17,000 values for O_2 cross sections in the Schumann-Runge band were calculated between 1753.52 Å and 1987.48 Å. The two techniques will be compared later.

3. CALCULATED PHOTODISSOCIATION RATES

3.1 Carbon Monoxide (CO)

Although the dissociation region for CO goes from the ionization limit at 885.6 Å to the dissociation limit at 1115.8 Å, cross-section measurements [Myer and Sampson, 1970] are available only for wavelengths longer than 1050 Å, or less than one-third of the total wavelength region. However, as discussed earlier, calculations for wavelengths short of 1027.5 Å are of little phyical interest so the only missing cross sections that are important are those for 24.5 Å. These cross sections are shown in Figure 6. They are moderately structured, typically $\sim 4 \times 10^{19} cm^2$, but increasing with decreasing wavelength. There are two strong (5×10^{-18} cm^2) absorption peaks evident in the cross sections, and one of these is almost exactly coincident with the NII solar line group at 1085 Å [Hinteregger, 1970].

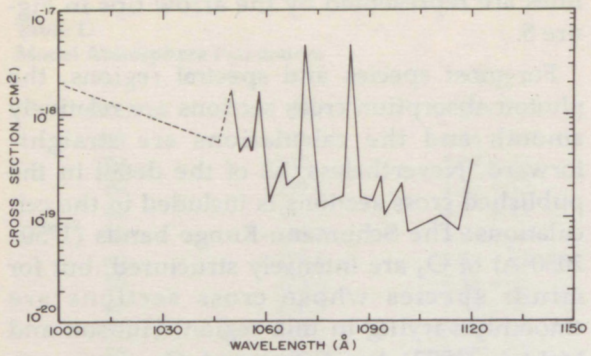

Figure 6. Experimental dissociation cross section of CO as a function of wavelength.

The calculated CO dissociation rates as a function of altitude parametric in solar zenith angle are shown in Figure 7. The low-zenith-angle curves show some slight structure that results from the coincidence of the absorption peak with the 1085 Å solar line. This is shown in detail in Figure 8 where the contribution from the line has been separated from the rest of the solar flux (labeled "band") for the overhead Sun. The 1085 Å line dominates the dissociation down to 100 km whereas below 100 km the line is absorbed strongly and the dissociation is determined by the rest of the solar spectrum.

To examine the effect of the missing cross sections below 1050 Å, an extrapolation (shown in Figure 6 as a dashed line) has been included in some of the calculations. This extrapolation has no physical basis, and should be considered only as indicative of the possible effect of the missing cross sections.

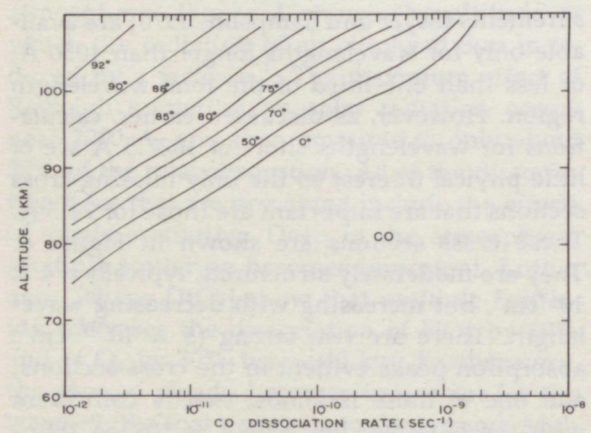

Figure 7. Dissociation rate per molecule of CO as a function of altitude with solar zenith angle parametric.

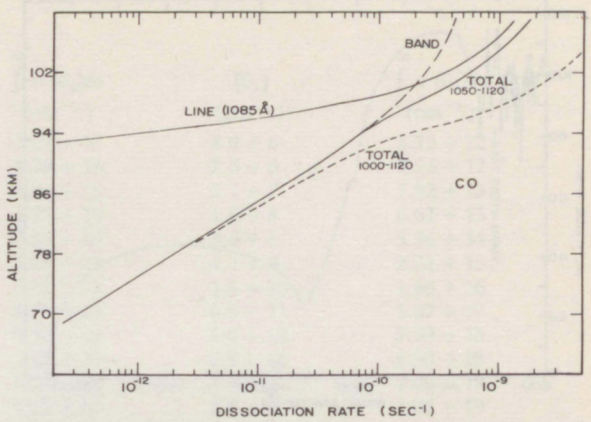

Figure 8. Contributions from various wavelength regions to the total dissociation rate of CO for an overhead Sun.

The effect of including the extrapolated (down to 1000 Å) cross sections is shown as a dashed line in Figure 8 for an overhead Sun. Such an inclusion raises the total dissociation rate noticeably above 80 km, and the extra dissociation rate dominates the total above 95 km. Clearly it would be useful to have measurements of the dissociation cross sections for CO in the region below 1050 Å. The variation of the dissociation rates with zenith angle at selected altitudes is shown in Figure 9. These curves contain the same data as those in Figure 8, but are plotted differently to facilitate interpolation.

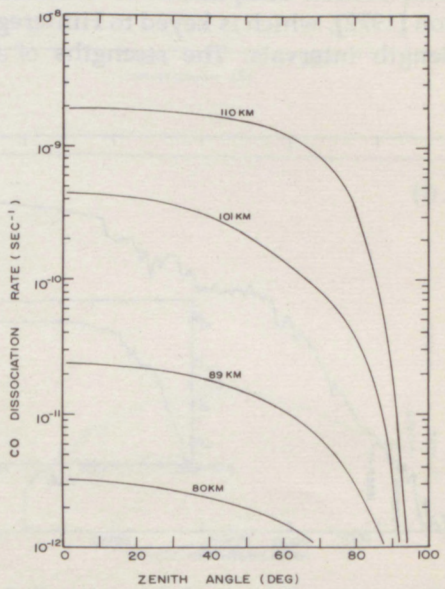

Figure 9. Dissociation rate per molecule of CO as a function of solar zenith angle with altitude parametric.

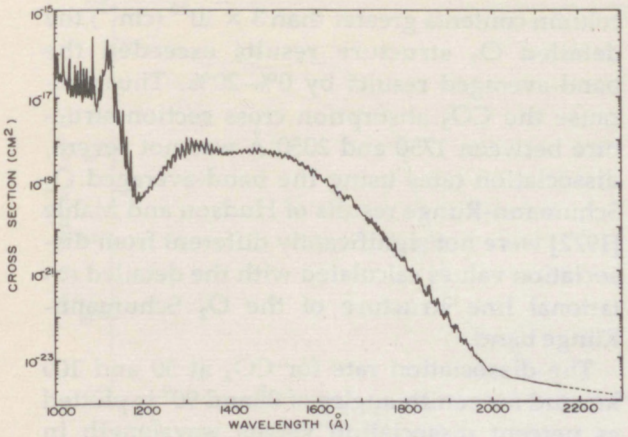

Figure 10. Experimental dissociation cross section of CO_2 as a function of wavelength.

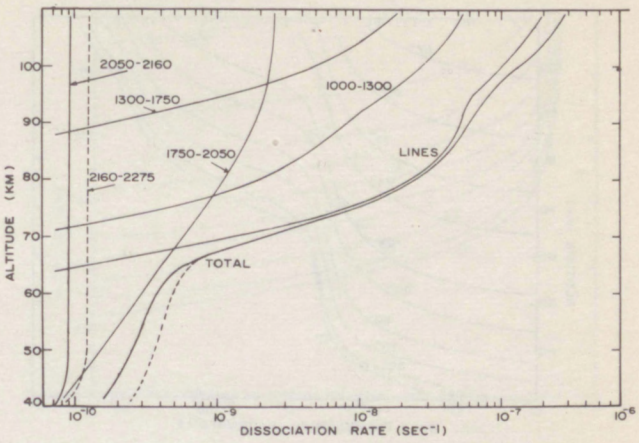

Figure 11. Contributions from various wavelength regions to the total dissociation rate of CO_2 for an overhead Sun.

3.2 Carbon Dioxide (CO_2)

Dissociation of CO_2 begins at the dissociation limit 2272.9 Å and continues through the ionization energy at 900.2 Å, although, as discussed before, calculations were carried down only to 1000 Å. Absorption cross sections for CO_2 were taken from Nakata et al. [1965] (1000–1100 Å), Inn et al. [1953] (1100–1718 Å), and Ogawa [1971] (1718–2160 Å) (Fig. 10). The region from 1000 to 1200 Å is strongly structured, as are the O_2 cross sections. Calculations utilizing all of the detailed structure have been made, but it is found that dissociation in the 1000–1300 Å range is dominated by the solar lines as indicated in Figure 11. No cross-section measurements appear to exist between 2160 Å and the dissociation limit at 2272.9 Å, but cross sections in the region adjacent are sufficiently small that this omission should cause no difficulty except at the lower altitudes. To examine this point, an extrapolation of the cross sections through the 2160–2273 Å region have been made as indicated by the dashed line in Figure 10. This extrapolation has no physical basis, and its effects should be considered only as indicative of possible effects from this region.

The contributions to the dissociation rate from the various wavelength regions are shown in Figure 11. The solar lines dominate the dissociation rate down to 66 km; here the Schumann-Runge bands (1750–2050 Å) penetrate and cause the sharp turnover in the dissociation rate profile. The extrapolated 2160–2273 Å region also becomes significant in this region. (The dashed "total" line includes the extrapolated region; the solid "total" line does not.)

The variation of the total photodissociation rate profile with zenith angle (not including the extrapolated region) is shown in Figure 12. Notice that the variation of the dissociation rate for a zenith angle variation from 0° is much larger above 60 km than below. The variation of dissociation rate with zenith angle, parametric in altitude, is shown in Figure 13. The dissociation rate curves for CO_2 shown above were based on averaging the CO_2 cross sections in the 19 wavelength intervals specified by Hudson and Mahle [1972] for the O_2 Schumann-Runge bands between 1750 and 2050 Å. Figure 14 illustrates that in the 1750–2050 Å wavelength region average values for CO_2 cross sections can be chosen for the wave-length intervals specified by Hudson and Mahle [1972], and these average values differ by less than a factor of two from the measured values. Therefore, dissociation rates calculated from detailed CO_2 and O_2 cross sections should not greatly differ from dissociation rates calculated with the band-averaged results of Hudson and Mahle [1972]. Park's [1974] model of the Schumann-Runge band of O_2 was used to generate approximately 17,000 O_2 absorption cross sections. These values and the CO_2 cross sections of Figure 10 were used to recalculate the dissociation rate of CO_2. For small O_2 column densities less than 2×10^{20} the two methods yielded identical results. For column densities between 2×10^{20} and 3×10^{22} the j_{CO_2} values computed with the Park model Schumann-Runge absorption cross sections yielded dissociation rates 0%–20% lower than j_{CO_2} values utilizing the Hudson-Mahle band-averaged O_2 cross sections. For O_2

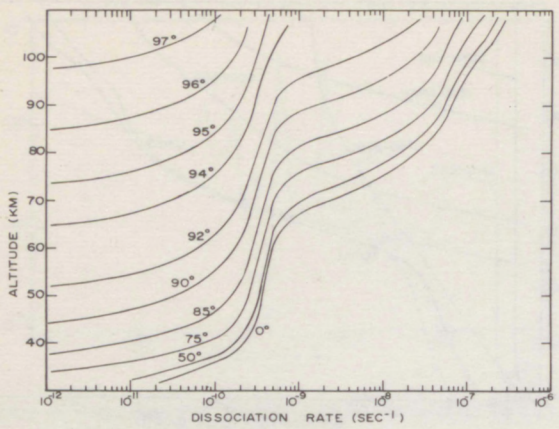

Figure 12. Dissociation rate per molecule of CO_2 as a function of altitude with solar zenith angle parametric.

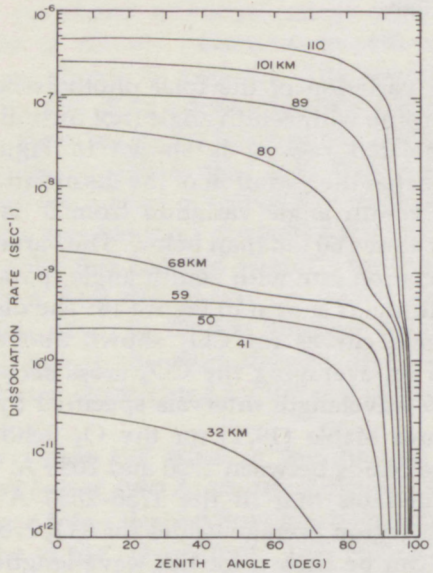

Figure 13. Dissociation rate per molecule of CO_2 as a function of solar zenith angle with altitude parametric.

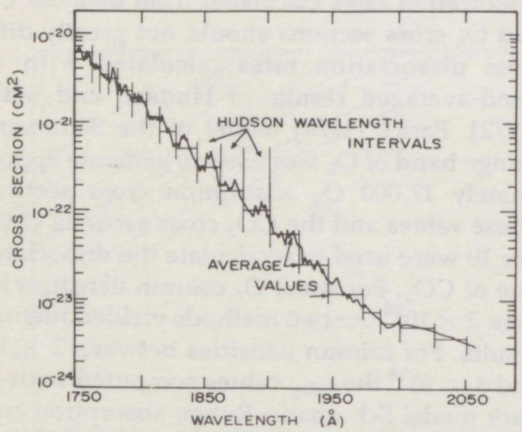

Figure 14. CO_2 absorption cross section in the O_2 Schumann-Runge band and associated band intervals for averaging from Hudson and Mahle [1972].

column contents greater than 3×10^{22} (cm^{-2}) the detailed O_2 structure results exceeded the band-averaged results by 0%–20%. Thus, because the CO_2 absorption cross section structure between 1750 and 2050 Å was not severe, dissociation rates using the band-averaged O_2 Schumann-Runge results of Hudson and Mahle [1972] were not significantly different from dissociation values calculated with the detailed rotational line structure of the O_2 Schumann-Runge band.

The dissociation rate for CO_2 at 50 and 100 km and for zenith angles of 0° and 90° is plotted as percent dissociation versus wavelength in Figure 15. At 100 km the major portion of the dissociation is produced by short 1000–1216 Å wavelengths whereas at 50 km the short wavelengths are gone and the dissociation is produced by 2000–2300 Å radiation.

3.3 Methane (CH_4)

The dissociation of methane begins at 2746 Å (4.40 eV), while the onset of ionization is at 961.7 Å (12.88 eV) [Chemical Rubber Co., 1975]. Data for the photoabsorption cross-sections were taken from Sun and Weissler [1955] (1000–1130 Å), Laufer and McNesby [1965] (1130–1440 Å), and Watanabe et al. [1953] (1440–1661 Å). We found no data for the 1611–1736 Å region. The cross sections vary smoothly with wavelength in the dissociation region (Fig. 16). As with most species that absorb strongly in the 1000–1400 Å region, the dissociation rate profile is dominated by the solar lines, principally the hydrogen Lyman alpha

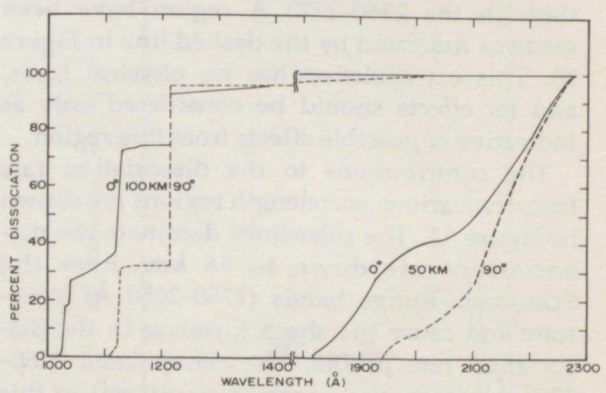

Figure 15. Percent dissociation of CO_2 versus wavelength for 50 and 100 km altitudes and for 0° and 90° zenith angles.

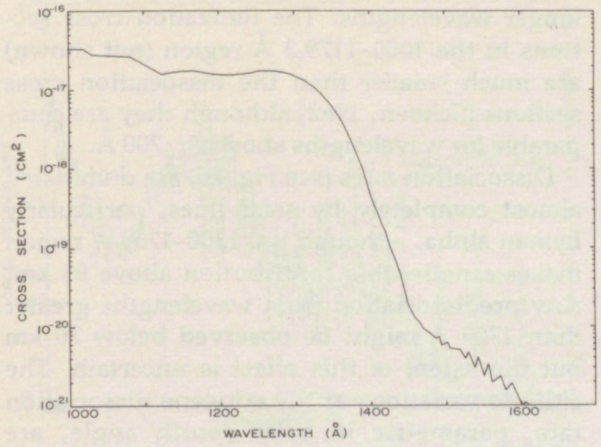

Figure 16. Experimental dissociation cross section of CH_4 as a function of wavelength.

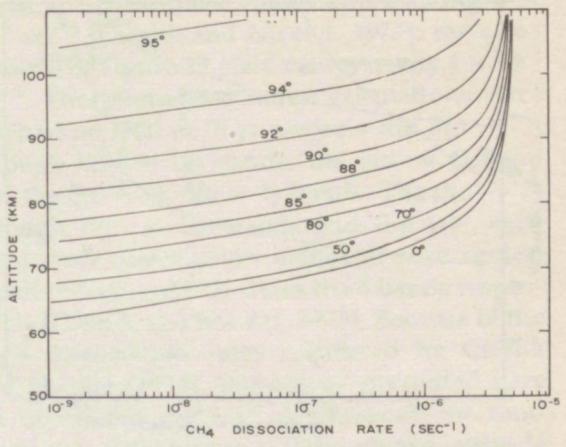

Figure 17. Dissociation rate per molecule of CH_4 as a function of altitude with solar zenith angle parametric.

line at 1215.7 Å. More than 99% of the dissociation rate values above 70 km are due to the Lyman alpha line. Since the dissociation rate is dominated so strongly by the solar lines, the variations are smooth and well-behaved (Fig. 17). The dissociation rate per molecule is 3–5 × 10^{-6} sec^{-1} down to ~80 km; it then falls rapidly and is effectively zero below 60 km. This gives a lifetime against dissociation of ~3 days at the higher altitudes for methane and even longer at lower altitudes. The variation of dissociation rate with zenith angle, parametric in altitude, is shown in Figure 18.

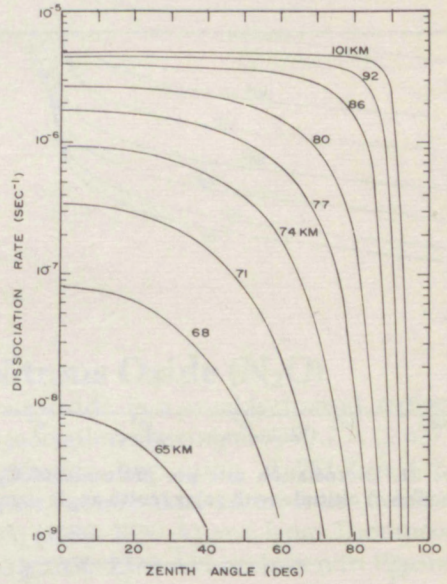

Figure 18. Dissociation rate per molecule of CH_4 as a function of solar zenith angle with altitude parametric.

3.4 Ethylene (C_2H_2)

The absorption spectrum for ethylene has been measured from 1970 Å down through the ionization limit at 1179.3 Å (10.52 eV). Data used here are taken from Schoen [1962] (1000–1240 Å) and Zelikoff and Watanabe [1953] (1240–1970 Å and are shown in Figure 19.

It is difficult to determine the exact dissociation threshold energy because of the large absorption peaks, similar to the Schumann-Runge bands of O_2 , at the onset of dissociation. Wilkinson and Mulliken [1955] estimate the dissociation energy at 7.26 eV (1709 Å) but do not discount the possibility of predissociation at

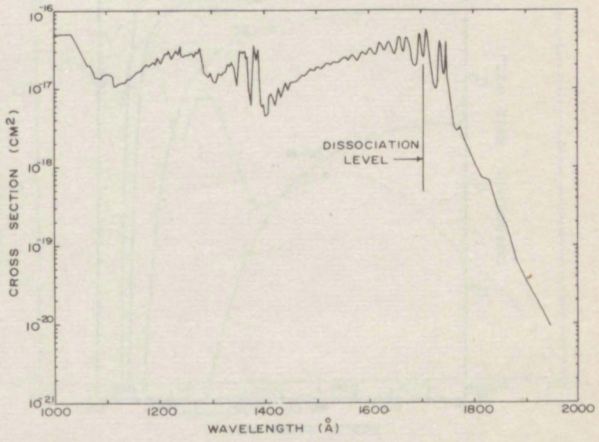

Figure 19. Experimental dissociation cross section of C_2H_2 as a function of wavelength.

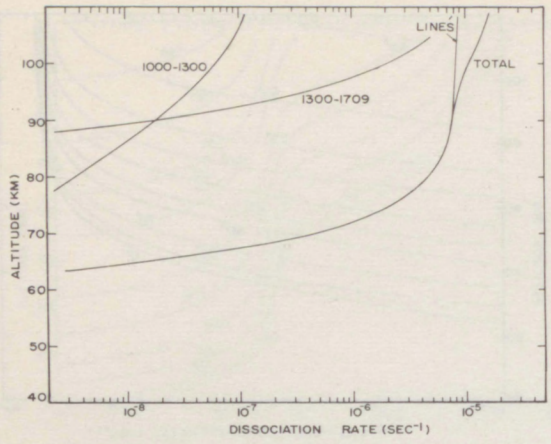

Figure 20. Contributions from various wavelength regions to the total dissociation rate of C_2H_2 for an overhead Sun.

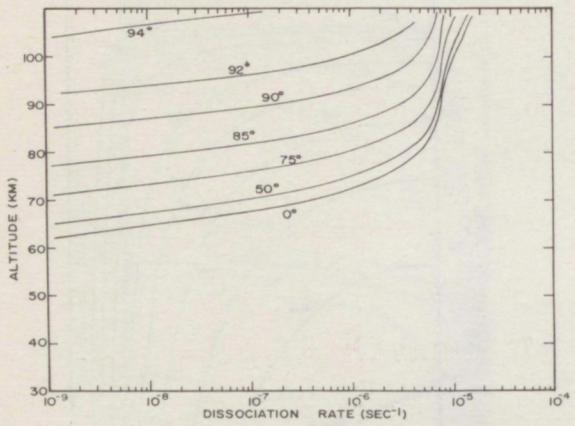

Figure 21. Dissociation rate per molecule of C_2H_4 as a function of altitude with solar zenith angle parametric.

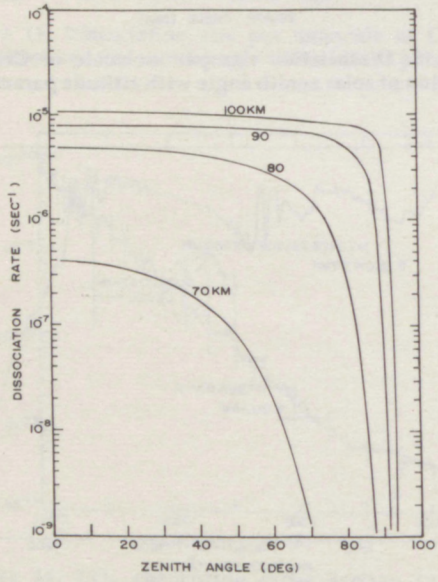

Figure 22. Dissociation rate per molecule of C_2H_4 as a function of solar zenith angle with altitude parametric.

longer wavelengths. The ionization cross sections in the 1000–1179.3 Å region (not shown) are much smaller than the dissociation cross sections [Schoen, 1962] although they are comparable for wavelengths short of ~700 Å.

Dissociation rates (see Fig. 20) are dominated almost completely by solar lines, particularly Lyman alpha, although the 1300–1709 Å region makes a noticeable contribution above 95 km. Any predissociation from wavelengths greater than 1709 Å might be observed below 70 km but the extent of this effect is uncertain. The altitude variations of the ethylene dissociation rate, parametric in solar zenith angle, are shown in Figure 21. For an overhead Sun, the dissociation rate falls effectively to zero below 60 km; for a 90° Sun, this altitude is raised to 85 km. These profiles, being dominated by the solar lines, show very little structure. The dissociation rate is 1×10^{-5} sec^{-1} at 100 km (implying a lifetime of about 1 day), but falls off rapidly at altitudes below 90 km. A plot of dissociation rate versus zenith angle, parametric in altitude, is shown in Figure 22.

3.5 Nitric Oxide (NO)

Of the absorption cross sections considered in this report, that of NO exhibits the greatest structure. The dissociation range of NO extends from the dissociation level 1908.4 Å (6.5 eV) down to the ionization level 1341 Å (9.25 eV). The ionization cross sections from Watanabe et al. [1967] (not shown) are smaller by a factor of 0.6–0.7 than the dissociation cross sections in the 1000–1341 Å region. The cross sections were taken from Watanabe et al. [1967] (1000–1350 Å) and Watanabe et al. [1953] (1350–1911 Å). An important part of the NO dissociation rate is produced by solar radiation of wavelength greater than 1750 Å. Of particular importance for this molecule is the predissociation that occurs in the δ bands, the $\beta(v' \geq 7)$ bands, and the $\gamma(v' \geq 4)$ bands. Cieslik and Nicolet [1973] have shown that the integrated absorption cross sections for the rotational lines of the δ(1–0) and δ(0–0) bands are as big as 2×10^{-16} (cm^2), whereas the NO absorption measurements cannot resolve the rotational line structure and thus yield averaged cross-section values that are only 10^{-18} cm^2 (see Fig. 23). Photodissociation rates based on the detailed rota-

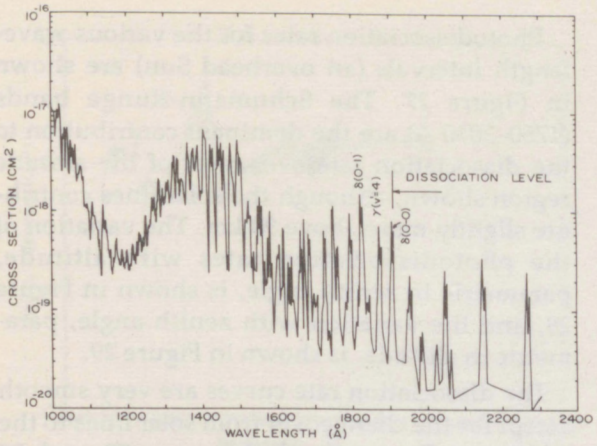

Figure 23. Experimental dissociation cross section of NO as a function of wavelength.

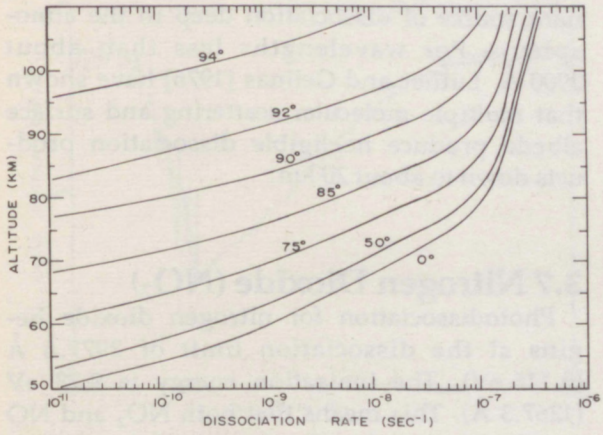

Figure 24. Dissociation rate per molecule of NO as a function of altitude with solar zenith angle parametric.

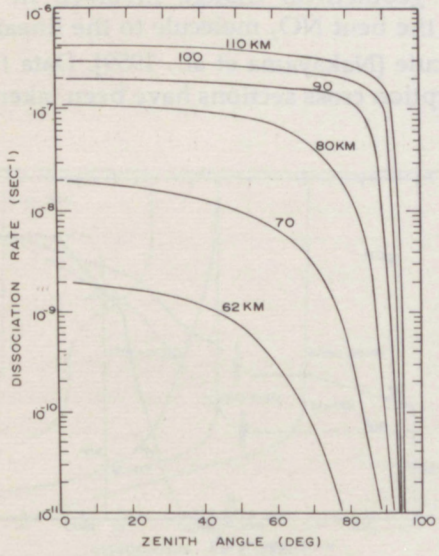

Figure 25. Dissociation rate per molecule of NO as a function of solar zenith angle with altitude parametric.

tional structure have values approaching 6×10^{-6} sec^{-1} [Cieslik and Nicolet, 1973]; the cross sections of Figure 23 yield values nearly 4×10^{-7} sec^{-1}. The photodissociation calculations were stopped at 1800 Å; this neglects the $\beta(v' = 7)$ through $\beta(v' = 10)$ bands, the $\gamma(v' = 4)$ band and the $\delta(v = 0)$, $\delta(v = 1)$ bands. The $\beta(v' = 7)$ through $\beta(v' = 10)$ bands and the $\gamma(v' = 4)$ band have dissociation values at zero optical depth of 0.02 and 0.01 times the δ bands respectively [Cieslik and Nicolet, 1973]. Because of the large dissociation rates calculated by Cieslik and Nicolet [1973], the curves presented here are of limited use but are included for completeness. Dissociation rates versus altitude and zenith angle are plotted in Figures 24 and 25.

3.6 Nitrous Oxide (N_2O)

Nitrous oxide is a weakly bound molecule, with dissociation starting at 7390.7 Å (1.677 eV) and ionization beginning at 961.2 Å (12.894 eV). Cross-section data taken from Zelikoff et al. [1953] (1080–2050 Å) and from Thompson et al. [1963] (2050–2390 Å) are shown in Figure 26. Cross sections for longer wavelengths are essentially zero [Johnston and Selwyn, 1975].

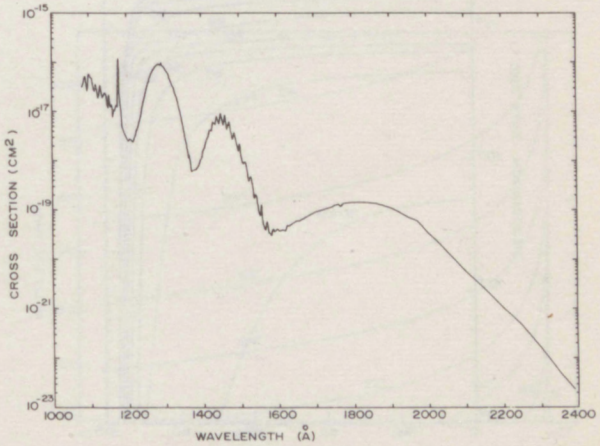

Figure 26. Experimental dissociation cross section of N_2O as a function of wavelength.

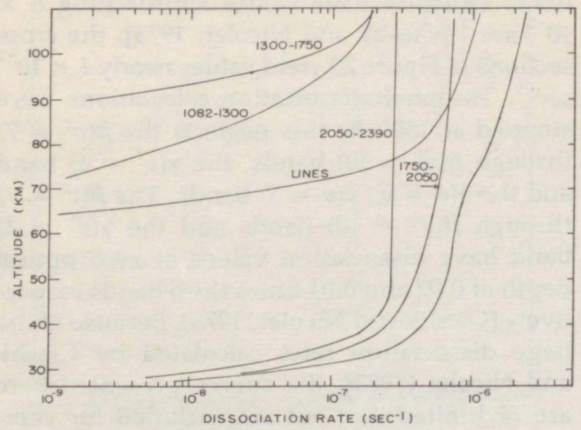

Figure 27. Contributions from various wavelength regions to the total dissociation rate of N_2O for an overhead Sun.

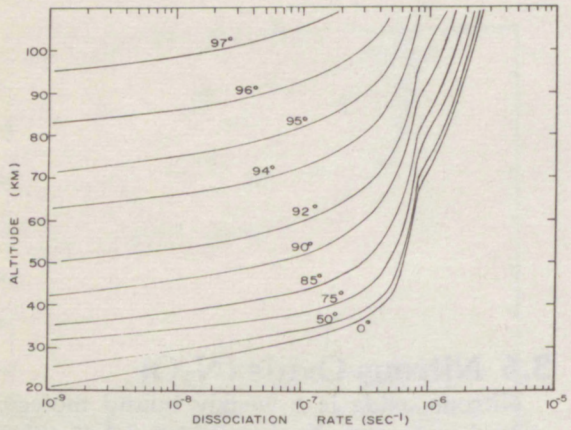

Figure 28. Dissociation rate per molecule of N_2O as a function of altitude with solar zenith angle parametric.

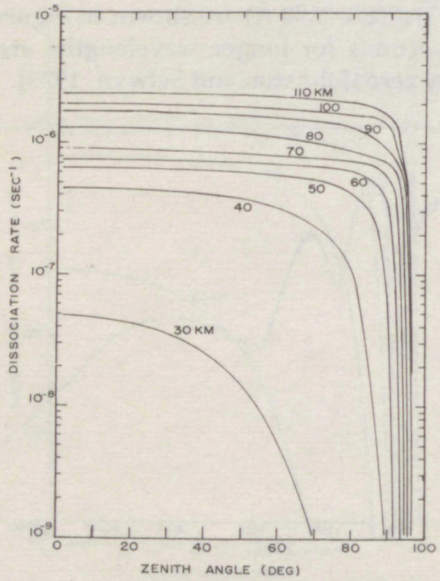

Figure 29. Dissociation rate per molecule of N_2O as a function of solar zenith angle with altitude parametric.

Photodissociation rates for the various wavelength intervals (an overhead Sun) are shown in Figure 27. The Schumann-Runge bands (1750–2050 Å) are the dominant contribution to the dissociation rate over most of the altitude region shown, although the solar lines contribute slightly more above 90 km. The variation of the photodissociation rates with altitude, parametric in zenith angle, is shown in Figure 28, and the variation with zenith angle, parametric in altitude, is shown in Figure 29.

The dissociation rate curves are very smooth except for the changeover from solar lines to the Schumann-Runge bands between 70 and 90 km. Figure 30 illustrates the percent dissociation versus wavelength for N_2O. It is apparent that the long wavelengths become the dominant source of dissociation deep in the atmosphere. For wavelengths less than about 2900 Å, Luther and Gelinas [1976] have shown that multiple molecular scattering and surface albedo produce negligible dissociation products down to about 20 km.

3.7 Nitrogen Dioxide (NO_2)

Photodissociation for nitrogen dioxide begins at the dissociation limit of 2977.6 Å (3.116 eV). The ionization energy is 9.78 eV (1267.3 Å). This means that both NO_2 and NO can be ionized by the Lyman alpha line at 1215.7 Å. However, NO_2 has a very low transition probability for ionization, because of the large geometrical change involved in going from the bent NO_2 molecule to the linear NO_2^+ molecule [Nakayama et al., 1959]. Data for the absorption cross sections have been taken from

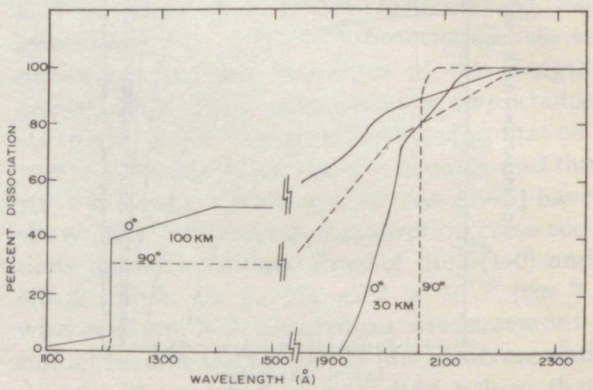

Figure 30. Percent dissociation of N_2O versus wavelength for 30 and 100 km altitudes and for 0° and 90° zenith angles.

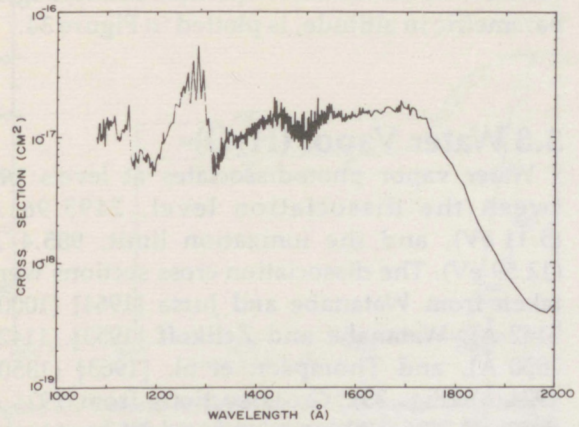

Figure 31a. Experimental NO_2 dissociation cross section from 1000 to 2000 Å.

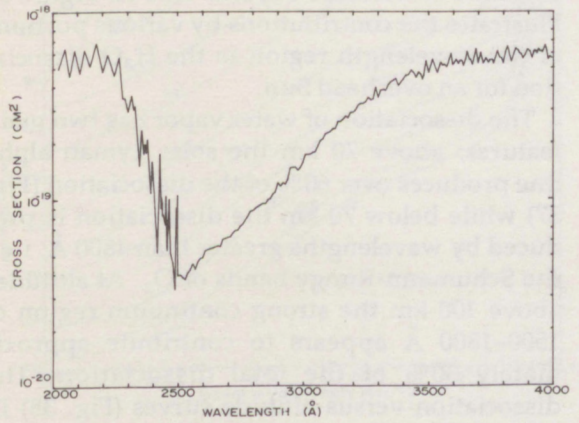

Figure 31b. Experimental NO_2 dissociation cross section from 2000 to 4000 Å.

Nakayama et al. [1959] (1080–2400 Å) and Hall and Blacet [1952] (2400–3977.6 Å). Apparently, no absorption data exist for the 1000–1080 Å region. Since there is ionization in the 1080–1267. 3 Å region, ionization cross sections have been subtracted so that the cross sections shown in Figures 31a and 31b are only for photodissociation. (The ionization cross section is 20% of the total at 1080 Å and less at longer wavelengths.)

The resultant dissociation rates from different spectral regions as a function of altitude are shown in Figure 32. The 2500–3977.6 Å region clearly contributes the majority of the dissociation products. As is true of most molecules with significant absorption in the visible, NO_2 has a high dissociation rate all the way to the ground. In fact, because solar flux in the 3000–4000 Å region can penetrate to the ground, molecular multiple scattering and surface albedo become important in the lower atmosphere. Luther and Gelinas [1976] have shown that multiple scattering increases the dissociation rate between 40 km and 50 km by 40%, and reflection from the ground increases it an additional 0%–60% depending on the surface albedo. These effects are zenith angle dependent however, and are negligible for angles greater than 90°. Our dissociation rates, including only single scattering events, were calculated down to 40 km (Fig. 33), but in view of Luther and Gelinas's results the values below 50 km may be somewhat in error. NO_2 has the largest dissociation rate of any species covered in this study–a value of 1×10^{-2} sec^{-1}, implying a lifetime against photodissociation of approximately 100 seconds. The

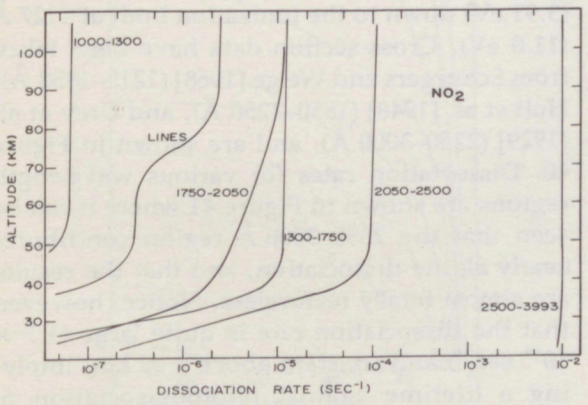

Figure 32. Contributions from various wavelength regions to the total dissociation rate of NO_2 for an overhead Sun.

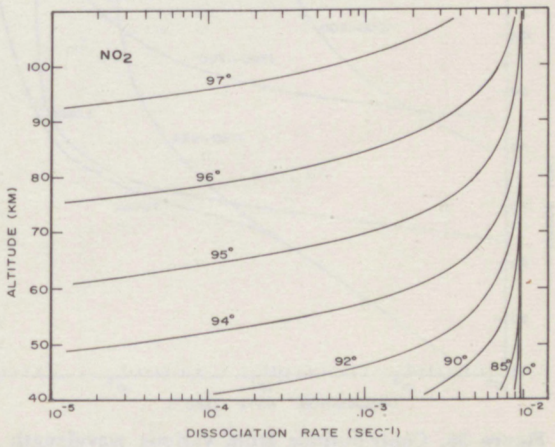

Figure 33. Dissociation rate per molecule of NO_2 as a function of altitude with solar zenith angle parametric.

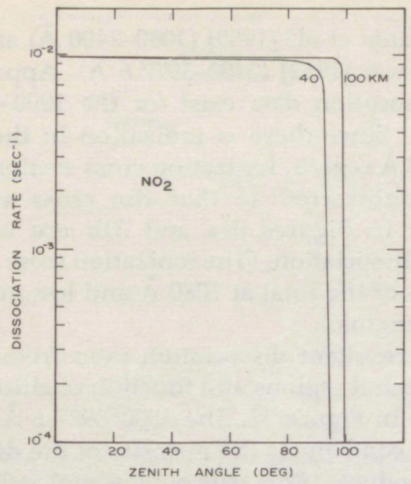

Figure 34. Dissociation rate per molecule of NO_2 as a function of solar zenith angle with altitude parametric.

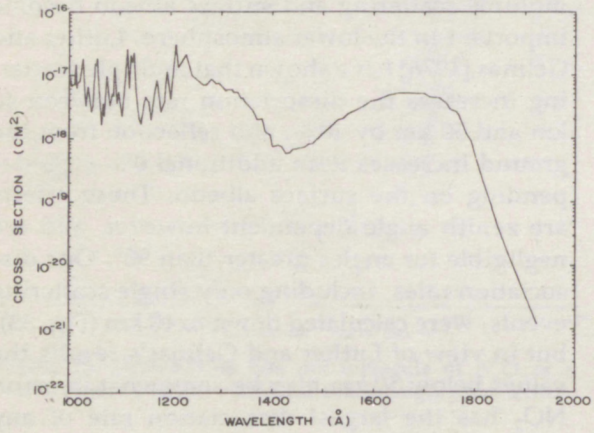

Figure 35. Experimental dissociation cross section of H_2O as a function of wavelength.

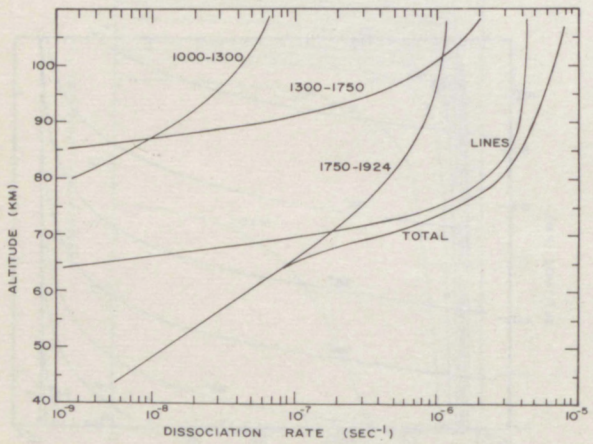

Figure 36. Contributions from various wavelength regions to the total dissociation rate of H_2O for an overhead Sun.

variation of dissociation rate with zenith angle, parametric in altitude, is plotted in Figure 34.

3.8 Water Vapor (H_2O)

Water vapor photodissociates at levels between the dissociation level, 2495.96 Å (5.11 eV), and the ionization limit, 985.4 Å (12.59 eV). The dissociation cross sections were taken from Watanabe and Jursa [1964] (1000–1142 Å), Watanabe and Zelikoff [1953] (1142–1850 Å), and Thompson et al. [1963] (1850–1924 Å) (Fig. 35). Cross sections from 1924 Å through 2426 Å apparently have not been measured in detail, but Thompson et al. [1963] and Anderson [1971] estimate that the cross sections continue to decrease beyond 1924 Å. Figure 36 illustrates the contributions by various portions of the wavelength region to the H_2O dissociation for an overhead Sun.

The dissociation of water vapor has two main features; above 70 km the solar Lyman alpha line produces over 60% of the dissociation (Fig. 37) while below 70 km the dissociation is produced by wavelengths greater than 1800 Å, i.e., the Schumann-Runge bands of O_2. At altitudes above 100 km the strong continuum region of 1500–1800 Å appears to contribute approximately 30% of the total dissociation. The dissociation-versus-altitude curves (Fig. 38) illustrate the smooth transition from one wavelength region to the other. Figure 39 gives the dissociation rate versus zenith angle for constant altitudes.

3.9 Hydrogen Peroxide (H_2O_2)

Hydrogen peroxide dissociates from 3173 Å (3.91 eV) down to the ionization limit at 1127 Å (11.0 eV). Cross-section data have been taken from Schurgers and Welge [1968] (1212–1850 Å), Holt et al. [1948] (1850–2250 Å), and Urey et al. [1929] (2250–3000 Å), and are shown in Figure 40. Dissociation rates for various wavelength regions are shown in Figure 41 where it can be seen that the 2050–3000 Å region contributes nearly all the dissociation, and that the results are almost totally featureless. Notice, however, that the dissociation rate is quite large (1.7×10^{-4} sec^{-1}) and constant above ~40 km, implying a lifetime against photodissociation of 5.9×10^3 seconds (100 minutes). At 30 km, over 70% of the dissociation is produced by

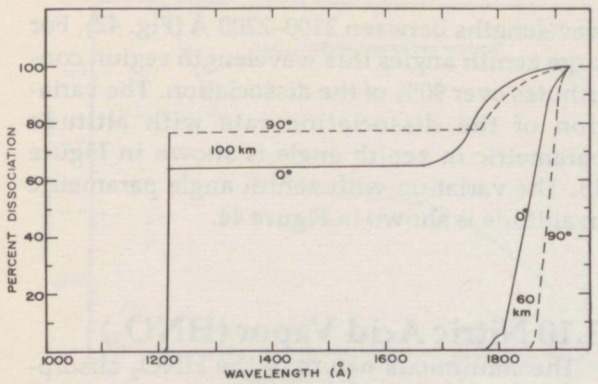

Figure 37. Percent dissociation of H_2O versus wavelength for 60 and 100 km altitudes and for 0° and 90° zenith angles.

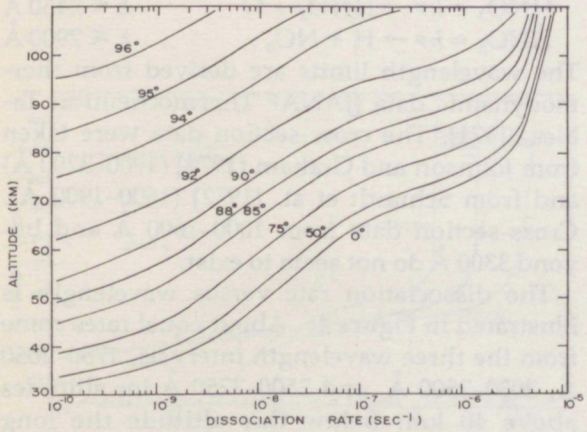

Figure 38. Dissociation rate per molecule of H_2O as a function of altitude with solar zenith angle parametric.

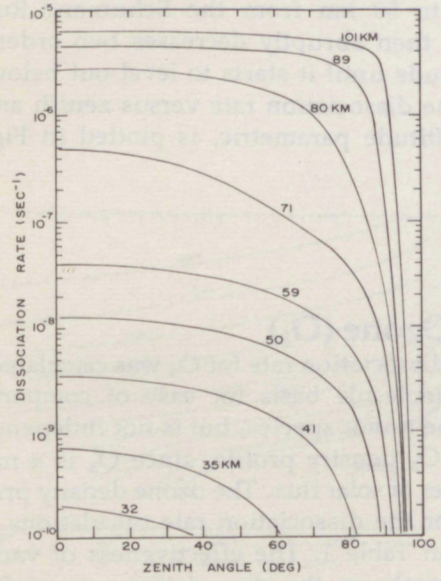

Figure 39. Dissociation rate per molecule of H_2O as a function of solar zenith angle with altitude parametric.

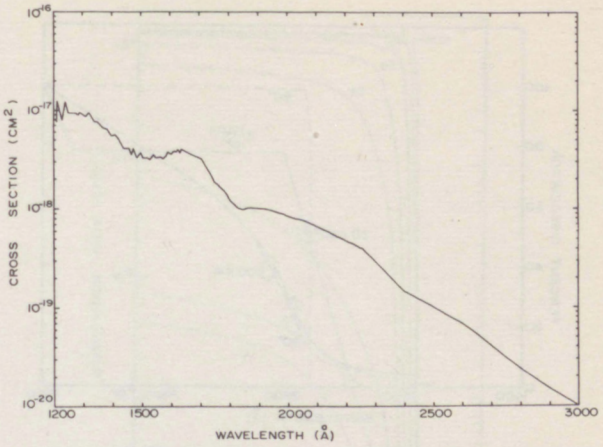

Figure 40. Experimental dissociation cross section of H_2O_2 as a function of wavelength.

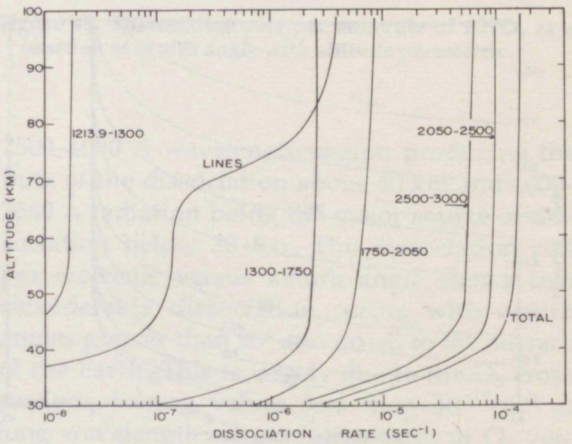

Figure 41. Contributions from various wavelength regions to the total photodissociation rate of H_2O_2 for an overhead Sun.

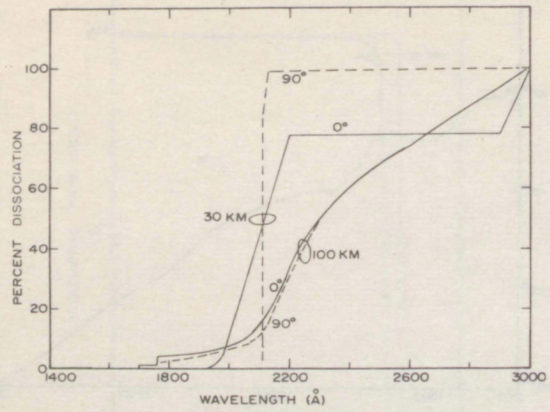

Figure 42. Percent dissociation of H_2O_2 versus wavelength for 30 and 100 km altitudes and for 0° and 90° zenith angles.

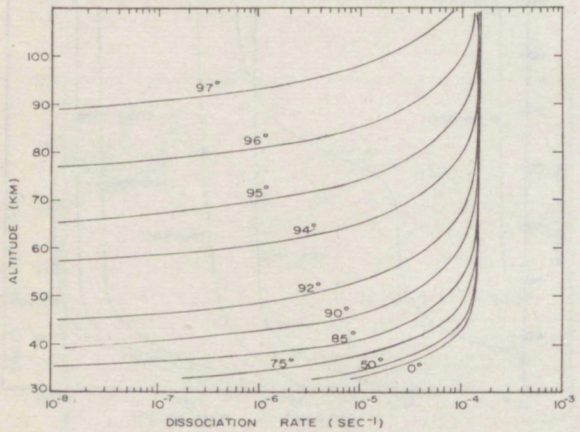

Figure 43. Dissociation rate per molecule of H_2O_2 as a function of altitude with solar zenith angle parametric.

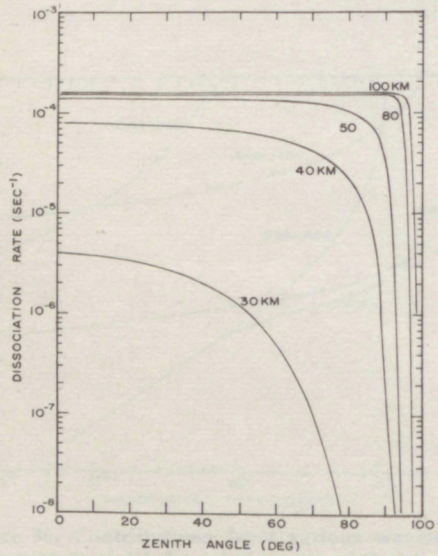

Figure 44. Dissociation rate per molecule of H_2O_2 as a function of solar zenith angle with altitude parametric.

wavelengths between 2100–2200 Å (Fig. 42). For large zenith angles this wavelength region contributes over 90% of the dissociation. The variation of the dissociation rate with altitude parametric in zenith angle is shown in Figure 43. The variation with zenith angle parametric in altitude is shown in Figure 44.

3.10 Nitric Acid Vapor (HNO_3)

The continuous nature of the HNO_3 absorption spectrum (Fig. 45) suggests that photodissociation is taking place. Three energetically possible reactions are the following:

$HNO_3 + h\nu \rightarrow HO + NO_2$ $\quad \lambda \leq 5980$ Å

$HNO_3 + h\nu \rightarrow HNO_2 + O$ $\quad \lambda \leq 2450$ Å

$HNO_3 = h\nu \rightarrow H + NO_3$ $\quad \lambda \leq 2900$ Å

The wavelength limits are derived from thermodynamic data [JANAF Thermochemical Tables, 1971]. The cross-section data were taken from Johnson and Graham [1973] (1900–3200 Å) and from Schmidt et al. [1972] (1600–1900 Å). Cross-section data from 1000–1600 Å and beyond 3300 Å do not seem to exist.

The dissociation rate versus wavelength is illustrated in Figure 46. About equal rates come from the three wavelength intervals, 1750–2050 Å, 2050–2500 Å, and 2500–3250 Å for altitudes above 40 km. Below this altitude the long wavelength dissociation becomes dominant. Figure 47 shows the dissociation rate curves versus altitude with zenith angle parametric. The dissociation is approximately constant down to 50 km from the Schumann-Runge bands, then abruptly decreases two orders of magnitude until it starts to level out below 20 km. The dissociation rate versus zenith angle, with altitude parametric, is plotted in Figure 48.

3.11 Ozone (O_3)

The dissociation rate for O_3 was calculated on a per molecule basis for ease of comparison with the minor species, but is not independent of the O_3 density profile, since O_3 is a major absorber of solar flux. The ozone density profile used for the dissociation rate calculations was given in Table 1. The effectiveness of various wavelengths in the dissociation rate of O_3 is shown in Figure 49. Most of the dissociation is produced by the long wavelengths with the

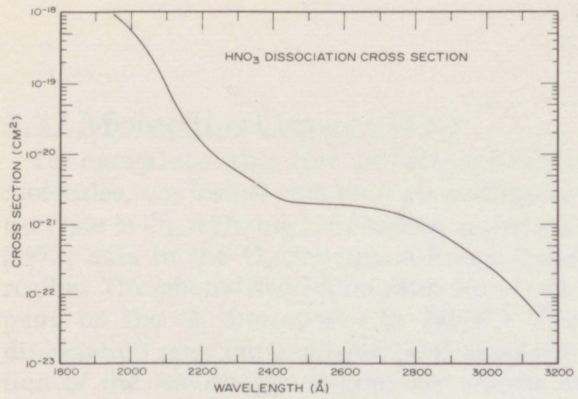

Figure 45. Experimental dissociation cross section of HNO_3 as a function of wavelength.

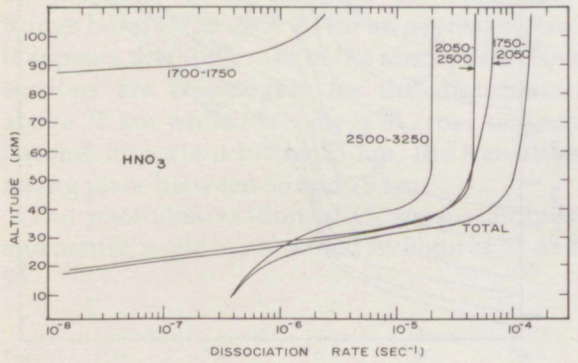

Figure 46. Contributions from the various wavelength regions to total photodissociation rate of HNO_3 for an overhead Sun.

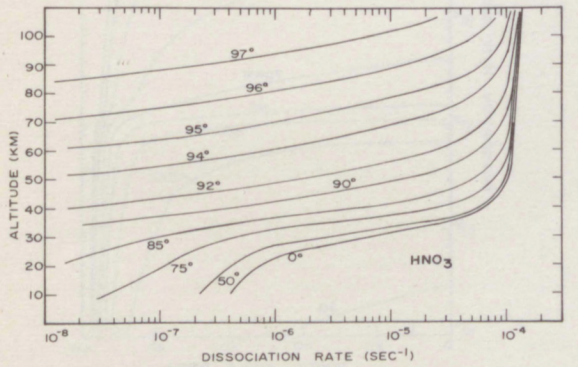

Figure 47. Dissociation rate per molecule of HNO_3 as a function of altitude with solar zenith angle parametric.

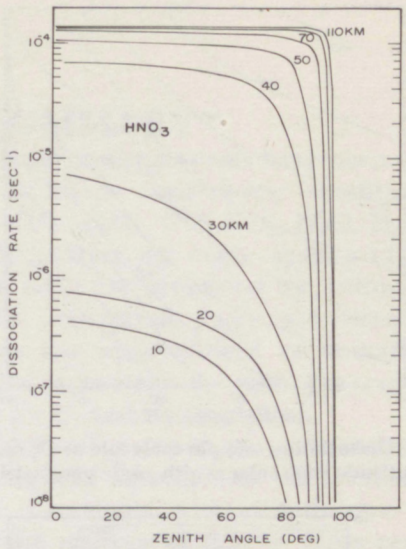

Figure 48. Dissociation rate per molecule of HNO_3 as a function of zenith angle with altitude parametric.

2500–4000 Å wavelength region producing the bulk of the dissociation above 40 km and 4000–7560 Å radiation being the major source of dissociation below 30 km. The dissociation rate per molecule versus zenith angle shows that considerable dissociation occurs with zenith angles greater than 90° and down to the surface of the Earth. This is largely due to the O_3 cross sections having values less than $10^{-19}cm^2$ at long wavelength. Dissociation rates of O_3 versus altitude, zenith angle as parameter, are shown in Figure 50. Rates versus zenith angle, altitude as parameter, are plotted in Figure 51.

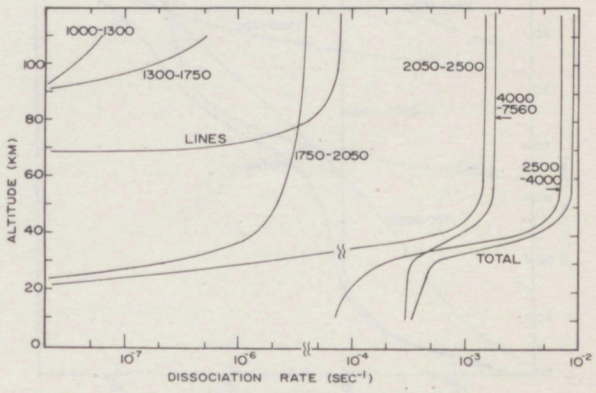

Figure 49. Contributions from various wavelength regions to the total dissociation rate of O_3 for an overhead Sun.

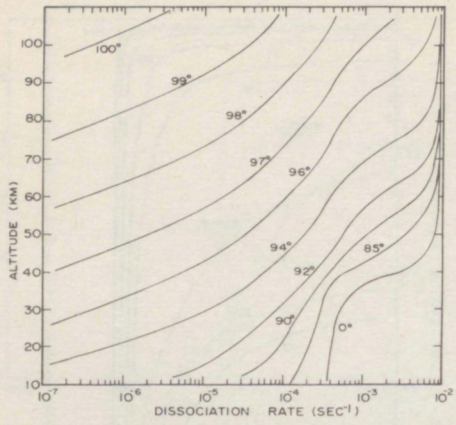

Figure 50. Dissociation rate per molecule of O_3 as a function of altitude with solar zenith angle parametric.

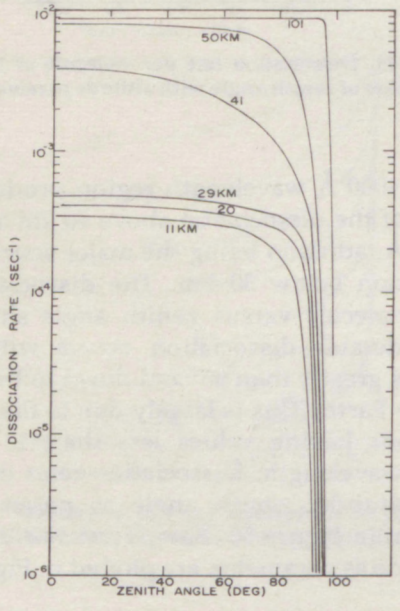

Figure 51. Dissociation rate per molecule of O_3 as a function of solar zenith angle with altitude parametric.

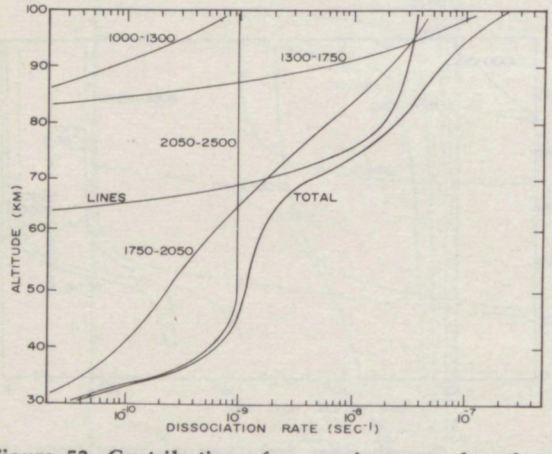

Figure 52. Contributions from various wavelength regions to the total dissociation rate of O_2 for an overhead Sun.

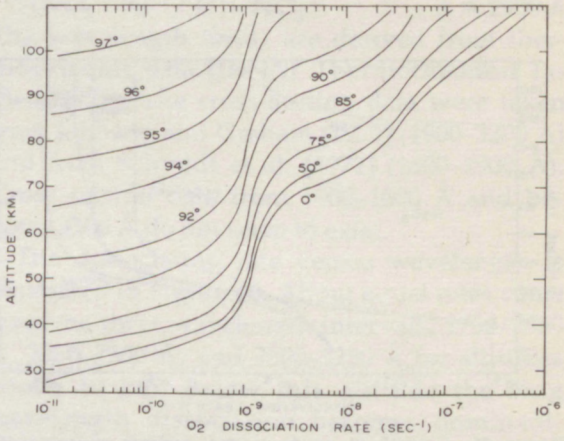

Figure 53. Dissociation rate per molecule of O_2 as a function of altitude with solar zenith angle parametric.

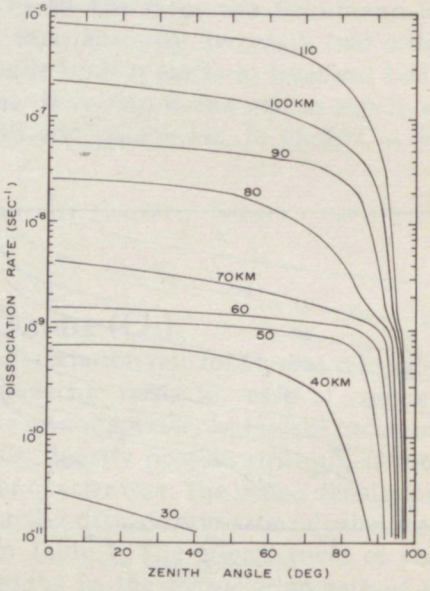

Figure 54. Dissociation rate per molecule of O_2 as a function of solar zenith angle with altitude parametric.

3.12 Molecular Oxygen (O_2)

To complete the list of atmospheric molecules, we include the total photodissociation rate of O_2, utilizing the Hudson and Mahle [1972] data in the O_2 Schumann-Runge band region. The photodissociation rates for O_2 depend on the O_2 atmosphere in Table 1. The dissociation rates (an overhead Sun) as a function of the wavelength regions are shown in Figure 52. Above 90 km the solar lines and the Schumann-Runge bands and continuum produce about equal parts of the dissociation products. Below 60 km the Herzberg continuum becomes the important source of photodissociation. An interesting feature is the unique shape of the curve for the Schumann-Runge band (1750–2050 Å) for an overhead Sun. It appears that the peaks of the absorption cross sections are responsible for the dissociation above 75 km while the valleys in cross sections become important below 55 km, the transition taking place between 55 and 75 km.

The photodissociation of O_2 versus altitude and zenith angle is presented in Figures 53 and 54.

4. SUMMARY

Photodissociation rates have been calculated for the minor atmospheric constituents CO, CO_2, CH_4, C_2H_4, NO, NO_2, N_2O, H_2O, H_2O_2, HNO_3 and for the major species O_2 and O_3. These rates are presented for altitudes below 110 km with zenith angle as a parameter. The curves are independent of specific minor species concentrations with the exception of those for O_2 and O_3 absorption.

Additional curves showing dissociation cross sections and dissociation rates versus zenith angle, parametric with altitude, are available from the authors. Computer cards can also be made available upon request.

5. ACKNOWLEDGMENTS

The Rayleigh scattering included in this work was prepared by Dr. L. R. Megill and his help is appreciatively acknowledged.

6. REFERENCES

Ackerman, M. (1971): Ultraviolet solar radiation related to mesospheric processes. In: *Mesospheric Models and Related Experiments*, G. Fiocco, ed., Reidel, Dordrecht, The Netherlands, 149–159.

Adams, G. W. and L. R. Megill (1970): SIXBIT, a generalized reaction kinetics program. ESSA Tech. Report ERL–177–SDL–15, Supt. of Documents, U.S. Government Printing Office, Washington, D.C. 20402.

Adams, G. W. (1974): Sources and sinks of energy in the lower thermosphere. NOAA Tech. Report ERL–304–SEL–28, Supt. of Documents, U.S. Government Printing Office, Washington, D.C. 20402.

Allen, C. W. (1963): *Astrophysical Quantities*. The Athlone Press, University of London.

Anderson, J. G. (1971): Rocket-borne ultraviolet spectrometer measurements of OH resonance fluorescence with a diffusive transport model for mesospheric photochemistry. *J. Geophys. Res.*, **76**, 4634–4651.

Chemical Rubber Co. (1975): *Handbook of Physics and Chemistry*, Cleveland, Ohio.

Cieslik, S. and M. Nicolet (1973): The aeronomic dissociation of nitric oxide. *Planet. Space Sci.*, **21**, 925–938.

Ditchburn, R. W. and P. A. Young (1962): The absorption of molecular oxygen between 1850 and 2500 Å. *J. Atmos. Terr. Phys.*, **24**, 127–139.

Donnelly, R. F. and J. H. Pope (1973): The 1–3000 Å solar flux for a moderate level of solar activity for use in modeling the ionosphere and upper atmosphere. NOAA Tech. Report ERL–276–SEL–25, Supt. of Documents, U.S. Govt. Printing Office, Washington, D.C. 20402.

Dutsch, H. U. and C. L. Mateer (1964): Uniform evaluation of Umkehr observations from the world ozone network, I, II, III. NCAR Tech. Notes, National Center for Atmospheric Research, Boulder, Colo. 80302.

Evans, W. F. J. (1967): Ph.D. Thesis, University of Saskatchewan.

Grobecker, A. J., ed. (1975): Natural stratosphere of 1974. CIAP Monograph 1, U.S. Department of Transportation, Washington, D.C.

Hall, T. C., Jr., and F. E. Blacet (1952): Separation of the absorption spectra of NO_2 and N_2O_4 in the range of 2400–5000 A. *J. Chem. Phys.*, **20**, 1745.

Hinteregger, H. E. (1970): The extreme ultraviolet solar spectrum and its variation during a solar cycle. *Ann. Geophys.*, **26**, 547.

Hinteregger, H.E., L. A. Hall, and G. Schmidtke (1965): Solar XUV radiation and neutral particle distribution in July 1963 thermosphere. In: *Space Research V*, North-Holland, Amsterdam, 1175.

Holt, R. B., C. K. McLane, and O. Oldenberg (1948): Ultraviolet absorption spectrum of hydrogen peroxide. *J. Chem. Phys.*, **16**, 225–229.

Hudson, R. D. (1971): Critical review of ultraviolet photoabsorption cross-sections for molecules of astrophysical and aeronomic interest. *Rev. of Geophys. and Space Phys.*, **9**, 305.

Hudson, R. D., and S. H. Mahle (1972): Interpolation constants for calculation of transmittance and rate of dissociation of molecular oxygen in the mesosphere and lower thermosphere. NASA Tech. Memo TM X–58084, NASA Manned Spaceflight Center, Houston, Texas.

Inn, Edward C. Y., K. Watanabe, and M. Zelikoff (1953): Absorption coefficients of gases in the vacuum ultraviolet, Part III, CO_2. *J. Chem. Phys.*, **21**, 1648–1650.

Inn, Edward C. Y., and Y. Tanaka (1959): Ozone absorption coefficients in the visible and ultraviolet regions. Presented at International Ozone Conference, Chicago, Ill., November, 1956; also in *Ozone Chemistry and Technology*, American Chemical Society, 1155 16th St. N.W., Washington, D.C., 263–368.

Jacchia, L. G. (1971): Revised static models of the thermosphere and exosphere with empirical temperature profiles. Special Report 332, Smithsonian Astrophysical Observatory, Cambridge, Mass.

JANAF Thermochemical Tables (1971): Report No. NSRDS–NBS–37, 2nd Ed., National Bureau of Standards, Washington, D.C.

Johnson, H., and R. Graham (1973): Gas-phase ultraviolet absorption spectrum of nitric acid vapor. *J. Phys. Chem.*, **77**, 62–63.

Johnston, H. S., and G. S. Selwyn (1975): New cross-sections for the absorption of near ultraviolet radiation by nitrous oxide (N_2O). *Geophys. Res. Letters*, **2**, 549–551.

Laufer, A. H., and J. R. McNesby (1965): Deuterium isotope effect in vacuum ultraviolet absorption coefficients of water and methane. *Can. J. Chemistry*, **43**, 3487–3490.

Luther, F. M., and R. J. Gelinas (1976): Effect of molecular scattering and surface albedo on atmospheric photodissociation rates. *J. Geophys. Res.*, **81**(6), 1125–1132.

Myer, J. A., and J. A. R. Samson (1970): Vacuum-ultraviolet absorption cross-sections of CO, HC1, and ICN between 1050 and 2100 Å. *J. Chem. Phys.*, **52**, 266–271.

Nakata, R. C., K. Watanabe, and F. M. Matsunaga (1965): Absorption and photoionization coefficients of CO_2 in the region 580–1670 Å. *Sci. of Light*, **14**, 54.

Nakayama, T., M. Y. Kitamura, and K. Watanabe (1959): Ionization potential and absorption coefficients of nitrogen dioxide. *J. Chem. Phys.*, **30**, 1180–1186.

Nicolet, M. (1975): Stratospheric ozone: An introduction to its study. *Rev. Geophys. Space Sci.*, **13,** 593–636.

Ogawa, M. (1971): Absorption cross sections of O_2 and CO_2 continua in the Schumann and far-uv regions. *J. Chem. Phys.*, **54,** 2550–2556.

Park, J. H. (1974): The equivalent mean absorption cross-sections for the O_2 Schumann-Runge bands: Application to the H_2O and NO photodissociation rates. *J. Atmos. Sci.*, **31,** 1893–1897.

Riegler, G. R., J. F. Drake, C. Liu, and R. J. Cicerone (1976): Stellar occultation measurements of atmospheric ozone and chlorine. *J. Geophys. Res.*, **81,** 4997–5012.

Shimazaki, T. and T. Ogawa (1974): A theoretical model of minor constituent distributions in the stratosphere including diurnal variations. *J. Geophys. Res.*, **79,** 3411–3423.

Schmidt, S. C., R. C. Amme, D. G. Murcray, A. Goldman, and F. S. Bonomo (1972): Ultraviolet absorption by nitric acid vapour. *Nature (London) Phys. Sci.*, **238,** 109.

Schoen, R. I. (1962): Absorption, ionization and ion-fragmentation cross-sections of hydrocarbon vapor under vacuum-ultraviolet radiation. *J. Chem. Phys.*, **37,** 2032–2042.

Schurgers, M. and K. H. Welge (1968): Absorptionskoeffizient von H_2O_2 und N_2H_4 zwischen 1200 und 2000 Å. *Z. Naturforsch.*, **23A,** 1508–1510.

Stolarski, R. S., and N. P. Johnson (1972): Photoionization and photoabsorption cross-sections for ionospheric calculations. *J. Atmos. Terr. Phys.*, **34,** 1691–1701.

Sun. H. and G. L. Weissler (1955): Absorption cross-sections of carbon dioxide and carbon monoxide in the vacuum ultraviolet. *J. Chem. Phys.*, **23,** 1625–1628.

Tanaka, Y., E. C. Y. Inn, and K. Watanabe (1953): Absorption coefficients of gases in the vacuum ultraviolet, Part IV, Ozone. *J. Chem. Phys.*, **21,** 1651–1653.

Thompson, B. A., P. Harteck, and R. R. Reeves, Jr. (1963): Ultraviolet absorption coefficients of CO_2, CO, O_2, H_2O, N_2O, NH_3, NO, SO_2, and CH_4 between 1850 and 4000 Å. *J. Geophys. Res.*, **68,** 6431–6436.

U.S. Standard Atmosphere (1962): Supt. of Documents, U.S. Govt. Printing Office, Washington, D.C. 20402.

Urey, H. C., L. H. Dawsey, and F. O. Rice (1929): The absorption spectrum and decomposition of hydrogen peroxide by light. *J. Am. Chem. Soc.*, **51,** 1371–1383.

Watanabe, K., M. Zelikoff, and E. C. Y. Inn (1953): Absorption coefficients of several atmospheric gases. AFCRL Tech. Rept. No. 53–23, Geophys. Res. Paper No. 21, Air Force Cambridge Research Center, L. G. Hanscom Field, Bedford, Mass. 01731.

Watanabe, K., and M. Zelikoff (1953): Absorption coefficients of water vapor in the vacuum ultraviolet. *J. Opt. Soc. Amer.*, **43,** 753–755.

Watanabe, K., and A. S. Jursa (1964): Absorption and photoionization cross-sections of H_2O and H_2S. *J. Chem. Phys.*, **41,** 1650–1653.

Watanabe, K., F. M. Matsunaga, and H. Sakai (1967): Absorption coefficient and photoionization yield of NO in the region 580–1350 Å. *App. Optics*, **6,** 391–396.

Wilkinson, P. G., and R. S. Mulliken (1955): Far ultraviolet absorption spectra of ethylene and ethylene-d4. *J. Chem. Phys.*, **23,** 1895–1907.

Wofsy, S. C. (1974): Atmospheric photochemistry of N, H, and C1 containing radicals. Third Conference on CIAP, U.S. Department of Transportation, A. J. Broderick and T. M. Hard, eds.

Zelikoff, M., and K. Watanabe (1953): Absorption coefficients of ethylene in the vacuum ultraviolet. *J. Opt. Soc. Amer.*, **43,** 756–759.

Zelikoff, M., K. Watanabe, and E. C. Y. Inn (1953): Absorption coefficients of gases in the vacuum ultraviolet, Part II, Nitrous oxide. *J. Chem. Phys.*, **21,** 1643–1647.

Environmental Research LABORATORIES

The mission of the Environmental Research Laboratories (ERL) is to conduct an integrated program of fundamental research, related technology development, and services to improve understanding and prediction of the geophysical environment comprising the oceans and inland waters, the lower and upper atmosphere, the space environment, and the Earth. The following participate in the ERL missions:

MESA *Marine EcoSystems Analysis Program.* Plans, directs, and coordinates the regional projects of NOAA and other federal agencies to assess the effect of ocean dumping, municipal and industrial waste discharge, deep ocean mining, and similar activities on marine ecosystems.

OCSEA *Outer Continental Shelf Environmental Assessment Program Office.* Plans and directs research studies supporting the assessment of the primary environmental impact of energy development along the outer continental shelf of Alaska; coordinates related research activities of federal, state, and private institutions.

W/M *Weather Modification Program Office.* Plans and coordinates ERL weather modification projects for precipitation enhancement and severe storms mitigation.

NHEML *National Hurricane and Experimental Meteorology Laboratory.* Develops techniques for more effective understanding and forecasting of tropical weather. Research areas include: hurricanes and tropical cumulus systems; experimental methods for their beneficial modification.

RFC *Research Facilities Center.* Provides aircraft and related instrumentation for environmental research programs. Maintains liaison with user and provides required operations or measurement tools, logged data, and related information for airborne or selected surface research programs.

AOML *Atlantic Oceanographic and Meteorological Laboratories.* Studies the physical, chemical, and geological characteristics and processes of the ocean waters, the sea floor, and the atmosphere above the ocean.

PMEL *Pacific Marine Environmental Laboratory.* Monitors and predicts the physical and biological effects of man's activities on Pacific Coast estuarine, coastal, deep-ocean, and near-shore marine environments.

GLERL *Great Lakes Environmental Research Laboratory.* Studies hydrology, waves, currents, lake levels, biological and chemical processes, and lake-air interaction in the Great Lakes and their watersheds; forecasts lake ice conditions.

GFDL *Geophysical Fluid Dynamics Laboratory.* Studies the dynamics of geophysical fluid systems (the atmosphere, the hydrosphere, and the cryosphere) through theoretical analysis and numerical simulation using powerful, high-speed digital computers.

APCL *Atmospheric Physics and Chemistry Laboratory.* Studies cloud and precipitation physics, chemical and particulate composition of the atmosphere, atmospheric electricity, and atmospheric heat transfer, with focus on developing methods of beneficial weather modification.

NSSL *National Severe Storms Laboratory.* Studies severe-storm circulation and dynamics, and develops techniques to detect and predict tornadoes, thunderstorms, and squall lines.

WPL *Wave Propagation Laboratory.* Studies the propagation of sound waves and electromagnetic waves at millimeter, infrared, and optical frequencies to develop new methods for remote measuring of the geophysical environment.

ARL *Air Resources Laboratories.* Studies the diffusion, transport, and dissipation of atmospheric pollutants; develops methods of predicting and controlling atmospheric pollution; monitors the global physical environment to detect climatic change.

AL *Aeronomy Laboratory.* Studies the physical and chemical processes of the stratosphere, ionosphere, and exosphere of the Earth and other planets, and their effect on high-altitude meteorological phenomena.

SEL *Space Environment Laboratory.* Studies solar-terrestrial physics (interplanetary, magnetospheric, and ionospheric); develops techniques for forecasting solar disturbances; provides real-time monitoring and forecasting of the space environment.

U.S. DEPARTMENT OF COMMERCE
National Oceanic and Atmospheric Administration
BOULDER, COLORADO 80302